IEEE Access
Multidisciplinary | Rapid Review | Open Access Journal

Received 23 November 2023, accepted 18 December 2023, date of publication 28 December 2023,
date of current version 16 January 2024.

Digital Object Identifier 10.1109/ACCESS.2023.3347738

RESEARCH ARTICLE

A Novel Optimization Method of Compensation Network Parameters for LCC Topology Wireless Power Transfer System With Anti-Offset Characteristics

YANG LU[1], DONGYUAN GE[2], LIAN MENG[3,4,5], CHUAN SUN[3,4,5], QI TANG[2], YILIN GAO[6], MENGMENG CHEN[1], AND CHENYANG XIA[1]

[1]Jiangsu Province Laboratory of Mining Electric and Automation, School of Electrical Engineering, China University of Mining and Technology, Xuzhou 221008, China
[2]State Grid Heilongjiang Information & Telecommunication Company Ltd., Harbin 150090, China
[3]State Grid Anhui Electric Power Company Ltd., Fuyang 236017, China
[4]Fuyang Power Supply Company, Fuyang 236017, China
[5]State Grid Corporation of China, Fuyang 236017, China
[6]School of Tourism and Hospitality Management, Hubei University of Economics, Wuhan 430205, China

Corresponding author: Yilin Gao (17184983@cumt.edu.cn)

This work was supported in part by the National Natural Science Foundation of China under Grant 52277020, and in part by the Natural Science Foundation of Jiangsu Province under Grant BK20211246.

ABSTRACT For the coil misalignment problem in the charging process of automatic guidance vehicles (AGVs), this paper proposes an optimization method for the bilateral LCC compensation network parameters based on quadruple-D quadrature (4DQ) coils. By introducing two coefficients K_T and K_{fl}, the compensation capacitors C_T and C_{fl} are optimized, achieving smaller output power fluctuations. Firstly, the capacitor values C_T and C_{fl} at resonance in the SS and PS equivalent circuit topology are obtained, meanwhile, the relationship between the output power P_{out} and the coupling coefficient k, represented by the coefficients K_T and K_{fl}, is obtained. Furthermore, with the transmission efficiency as the limiting condition, the output power fluctuation is effectively suppressed by adjusting K_T and K_{fl}. Finally, the experimental results show that after optimization the output power is 427.08W, and the transmission efficiency is 93.506% when the coupling coil are aligned, the system can still maintain a power output of at least 382.36W with a coil offset of 0-153mm in the X/Y axis directions, and the transmission efficiency is always above 89.472%. At the same time, the maximum deviation value ΔP_{abs_max} decreased from 213.1W before optimization to 111.0W after optimization, a decrease of 47.91%, effectively suppressing the power fluctuation and improving anti-offset performance.

INDEX TERMS AGV, 4DQ, bilateral LCC topology, compensation parameter optimization, anti-offset.

I. INTRODUCTION

Wireless power transmission (WPT) technology is increasingly being used in AGVs to ensure that the power supply system and AGVs are electrically and mechanically isolated, which in turn guarantees the uninterrupted operation of the AGVs and enhances the safety of the charging system [1], [2], [3], [4]. However, the misalignment of the receiving coil (Rx) and the transmitting coil (Tx) may cause voltage and current deviations, leading to severe fluctuations in the output power of the inductive power transfer (IPT) system [5], [6], [7]. To maintain the stability of the system, it is crucial to consider changes in the coupling mechanism's position and the corresponding value of mutual inductance drift. Nowadays, the methods often used to maintain the stability of the system output performance can be divided

The associate editor coordinating the review of this manuscript and approving it for publication was Tawfik Al-Hadhrami.

into the optimal design of magnetic coupling mechanisms, optimization measures of compensation topology, and control means [8], [9].

Magnetic coupling mechanism: reference [10] proposed a new magnetic coupling mechanism, which was based on the traditional square coil, the *Tx* coil extends its height in the vertical direction to form a solenoid-type magnetic circuit mechanism, although the coupling coefficient of the system has decreased, it has obtained excellent anti-offset capability. References [11] and [12] proposed adding a concentric plane coil in reverse series with the original *Tx* coil on *Tx* side, the *Tx* coil is a self-decoupled magnetic circuit structure formed by winding the magnetic circuit. When the deviation occurs, the coupling coefficients of the leading coil and the auxiliary coil with the *Rx* coil are reduced, respectively. The decreasing trend of the coupling coefficients of the two coils cancelled out each other by the connection form of reverse series connection, thus forming a strong anti-offset characteristic.

Circuit compensation topology: based on the opposite output characteristics of different circuit compensation structures cope with deflection, according to the resonance condition, the existing different circuit compensation structures can be efficiently combined, and the corresponding compensation circuit parameter values can be given, thus a new hybrid circuit compensation topology with anti-offset characteristics can be obtained [13]. Reference [14] proposed a hybrid compensation network structure based on an electric switch, which can control the on-off of the switch according to the deflection when the *Tx* coil adopts a ''Δ''-type magnetic structure and ''Y''-type magnetic structure respectively, the two schemes have different output characteristics under different deflections, which can be selected according to the specific deflection in actual working conditions. References [15] and [16] took S-CLC circuit compensation topology as an example, analyze the performance of the system based on particle swarm optimization algorithm, and provide a design method of compensation parameters. This method transforms the design problem of compensation network parameters into a multi-objective optimization problem. The main objective is to minimize the fluctuation of system output characteristics under deflection, and the parameters of compensation inductance and compensation capacitor are flexibly selected with consideration of the soft switching status.

Control strategy: reference [17] realized constant voltage output of secondary side by adding a Buck converter to the WPT system, but this approach will increase the transformed series of system power, resulting in unnecessary loss and reducing the efficiency of the system. Reference [18] improved the anti-offset performance by phase-shift control, but this method needed timely feedback signals from the secondary side of the system to be transmitted to the transmitting side in real-time, which was easy to cause time delay problems. Reference [19] proposed a frequency conversion control method based on a phase-locked loop. This method not only requires high-quality communication but also makes the input impedance angle of the WPT system too large during the control process, causing excessive voltage stress on the primary side. In addition, the control method is easy to increase the complexity and the overall energy cost [20], [21].

In summary, the above researches focus on the mutual inductance fluctuations between coupling mechanisms, requiring additional circuit compensation topologies or even complex control strategies, and the design of magnetic circuit mechanisms is also relatively complex. This article deduces and optimizes the compensation network parameters of the bilateral LCC equivalent circuit, constructs and studies the SS equivalent circuit topology and PS equivalent circuit topology, and correspondingly obtains the circuit compensation parameters represented by the adjustment coefficients K_{T} and K_{f1}, then obtains the expression between the system output power P_{out} and the coupling coefficient k represented by the adjustment coefficients K_{T} and K_{f1}, and study the effects of the adjustment coefficients K_{T} and K_{f1} on the output power P_{out}, respectively. By combining the limitations of the system transmission efficiency, the optimal combination of adjustment coefficients K_{T} and K_{f1} is obtained, ensuring that the system output power remains relatively stable within the wide range of coupling coefficient interval, thereby improving the anti-offset ability and transmission characteristics. Compared with other similar papers, the optimization scheme proposed in this paper not only maintains high system transmission efficiency and a constant output current on the receiving side, but also effectively suppresses output power fluctuations within a large offset range of the coupling mechanism by adjusting only two capacitor parameters.

II. OPTIMIZATION DESIGN OF COMPENSATION PARAMETERS FOR LCC-LCC TYPE IPT SYSTEMS

From complete alignment of the *Tx* and *Rx* coils to a gradual increase in the degree of offset, i.e., the coupling coefficient gradually decreases from the standard value, the output power of SS circuit topology shows an increasing trend with the decrease of mutual inductance, on the contrary, PS circuit topology presents a corresponding decreasing trend. The output power of SS and PS circuit topology shows an opposite trend with the decrease of mutual inductance. Therefore, based on the above characteristics, by optimizing the circuit topology compensation parameters and introducing two adjustment coefficients K_{T} and K_{f1}, the two circuit topology characteristics can be integrated into the bilateral LCC type IPT system to achieve smaller output power fluctuations and enhance the anti-offset ability of the IPT system.

As shown in Figure 1, in order to simplify the analysis, all passive components are ideal devices, ignoring the parasitic resistance of inductors and capacitors in the circuit. U_{p} is the fundamental output voltage of the inverter circuit, I_{Lf1} is the output fundamental phase current, and I_{T} and I_{R} are the

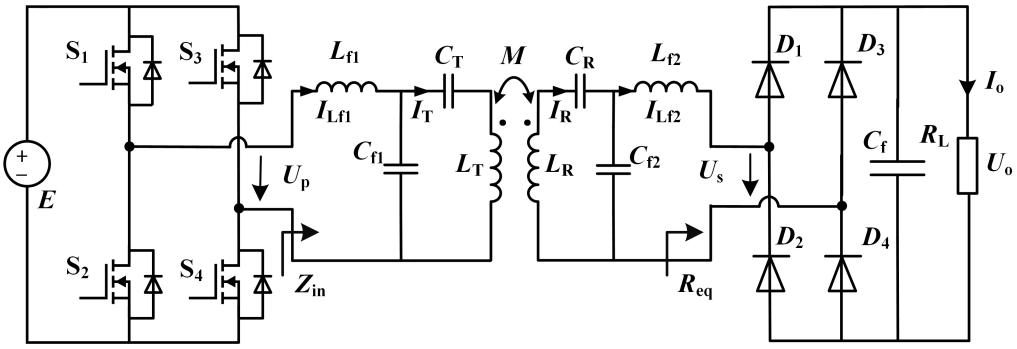

FIGURE 1. Schematic diagram of bilateral LCC resonant compensation circuit topology.

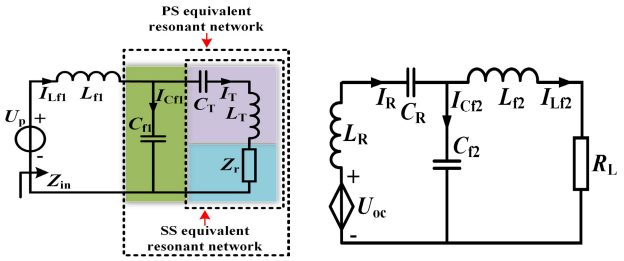

FIGURE 2. Equivalent schematic diagram of bilateral LCC resonant compensation circuit. (a) Primary side equivalent circuit; (b) Secondary side equivalent circuit.

phase currents flowing through the primary and secondary resonant coils, respectively, and I_{Lf2} is the phase current flowing through the load. Z_{in} is the input impedance. The primary LCC-type resonance compensation network is made up of compensating inductance L_{f1}, compensation capacitors C_{f1} and C_T, while the secondary network is made up of compensating inductance L_{f2}, compensation capacitors C_{f2} and C_R. L_T and L_R represent the resonant coils of the *Tx* and *Rx* coils. R_L is the DC load and R_{eq} is the equivalent AC load.

As shown in Figure 2, Z_r is the reflection impedance converted to the *Tx* side, $Z_r=(\omega M)^2/Z_S$, Z_S is the secondary impedance, U_{oc} is the open circuit voltage of the equivalent circuit on the secondary side, $\dot{U}_{oc}=j\omega M\dot{I}_T$, $R_{eq}=8R_L/\pi^2$. According to the KCL and KVL theorem, the following equation can be obtained:

$$\begin{cases} \dot{U}_p = \dot{I}_{Lf1}j\omega L_{f1} + \left(\dot{I}_{Lf1} - \dot{I}_T\right)\dfrac{1}{j\omega C_{f1}} \\ \dot{U}_p = \dot{I}_{Lf1}j\omega L_{f1} + \dot{I}_T\left(j\omega L_T + \dfrac{1}{j\omega C_T} + Z_r\right) \\ \dot{U}_{oc} = \dot{I}_R\left(j\omega L_R + \dfrac{1}{j\omega C_R}\right) + \left(\dot{I}_R - \dot{I}_{Lf2}\right)\dfrac{1}{j\omega C_{f2}} \\ \dot{U}_{oc} = \dot{I}_R\left(j\omega L_R + \dfrac{1}{j\omega C_R}\right) + \dot{I}_{Lf2}\left(j\omega L_{f2} + R_{eq}\right) \end{cases} \tag{1}$$

The input impedance Z_{in} of the *Tx* side and the equivalent impedance Z_S of the secondary side are as follows:

$$Z_{in} = j\omega L_{f1} + \left(j\omega L_T + \frac{1}{j\omega C_T} + Z_r\right) // \frac{1}{j\omega C_{f1}} \tag{2}$$

$$Z_S = j\omega L_R + \frac{1}{j\omega C_R} + \frac{1}{j\omega C_{f2}} // \left(j\omega L_{f2} + R_{eq}\right) \tag{3}$$

In the formula, the symbol // represents impedance parallel connection, $\omega = 2\pi f$, f is the switching frequency of the inverter. When both the *Tx* and *Rx* coils of the system are in a resonant state, the compensation parameters of each circuit meet the following relationship:

$$\begin{cases} \dfrac{1}{\omega_0^2} = L_{f1}C_{f1} \\ \dfrac{1}{\omega_0^2} = L_{f2}C_{f2} \\ \dfrac{1}{\omega_0^2} = (L_T - L_{f1})\,C_T \\ \dfrac{1}{\omega_0^2} = (L_R - L_{f2})\,C_R \end{cases} \tag{4}$$

The equivalent impedance of the secondary side, reflection impedance, and input impedance of the system under resonance conditions can be obtained by combining the above equation as follows:

$$\begin{aligned} Z_{S0} &= j\omega L_R - j\omega L_{f2} + j\omega L_{f2} + \frac{1}{j\omega C_R} + \frac{\frac{1}{j\omega C_{f2}}\left(j\omega L_{f2} + R_{eq}\right)}{R_{eq}} \\ &= \frac{L_{f2}}{R_{eq}C_{f2}} \end{aligned} \tag{5}$$

$$Z_{r0} = \frac{\omega_0^2 M^2 C_{f2} R_{eq}}{L_{f2}} \tag{6}$$

$$Y_{11} = \frac{1}{j\omega L_{f1}} \tag{7}$$

$$Z_{11} = j\omega L_{f1} \tag{8}$$

$$\dot{U}_{oc} = \frac{U_P M}{L_{f1}}\angle 0^0 \tag{9}$$

$$\begin{aligned} Z_{in0} &= j\omega L_{f1} + \left(j\omega L_T + \frac{1}{j\omega C_T} + Z_{r0}\right) // \frac{1}{j\omega C_{f1}} \\ &= j\omega L_{f1} + \left(j\omega L_T + \frac{1}{j\omega C_T} - j\omega L_{f1} + j\omega L_{f1} + Z_{r0}\right) // \frac{1}{j\omega C_{f1}} \\ &= j\omega L_{f1} + \left(j\omega L_{f1} + Z_{r0}\right) // \frac{1}{j\omega C_{f1}} \\ &= \frac{\omega_0^2 L_{f1}^2 L_{f2}^2}{M^2 R_{eq}} \end{aligned} \tag{10}$$

After simplification, the input current, output current, and resonant coil current of the T_x and R_x coils are as follows:

$$\dot{I}_{\mathrm{Lf1}} = U_{\mathrm{p}} \frac{M^2 R_{\mathrm{eq}}}{\omega_0^2 L_{\mathrm{f1}}^2 L_{\mathrm{f2}}^2} \angle 0^0 \tag{11}$$

$$\dot{I}_{\mathrm{T}} = U_{\mathrm{p}} \frac{1}{\omega_0 L_{\mathrm{f1}}} \angle -90^0 \tag{12}$$

$$\dot{I}_{\mathrm{R}} = U_{\mathrm{p}} \frac{M C_{\mathrm{f2}} R_{\mathrm{eq}}}{L_{\mathrm{f1}} L_{\mathrm{f2}}} \angle 0^0 \tag{13}$$

$$\dot{I}_{\mathrm{Lf2}} = U_{\mathrm{p}} \frac{M}{\omega_0 L_{\mathrm{f1}} L_{\mathrm{f2}}} \angle -90^\circ \tag{14}$$

In the resonant state, the input power and output power of the system are as follows:

$$P_{\mathrm{in}} = I_{\mathrm{Lf1}}^2 Z_{\mathrm{in0}} = \left(\frac{U_{\mathrm{p}} M^2 R_{\mathrm{eq}}}{\omega_0^2 L_{\mathrm{f1}}^2 L_{\mathrm{f2}}^2} \right)^2 \frac{\omega_0^2 L_{\mathrm{f1}}^2 L_{\mathrm{f2}}^2}{M^2 R_{\mathrm{eq}}} = \frac{U_{\mathrm{p}}^2 M^2 R_{\mathrm{eq}}}{\omega_0^2 L_{\mathrm{f1}}^2 L_{\mathrm{f2}}^2} \tag{15}$$

$$P_{\mathrm{out}} = I_{\mathrm{Lf2}}^2 R_{\mathrm{eq}} = \left(\frac{M U_{\mathrm{p}}}{\omega_0 L_{\mathrm{f1}} L_{\mathrm{f2}}} \right)^2 R_{\mathrm{eq}} = \left(\frac{k \sqrt{L_1 L_2} U_{\mathrm{p}}}{\omega_0 L_{\mathrm{f1}} L_{\mathrm{f2}}} \right)^2 R_{\mathrm{eq}} \tag{16}$$

Circuit parameters L_{T} and C_{T} form a LC series branch and are connected in series with the reflection impedance Z_{r}, which can be regarded as an equivalent SS topology. At the same time, the compensation capacitor C_{f1} is connected in parallel with the LC series branch mentioned above, which can be regarded as an equivalent PS topology. Therefore, the LCC-type resonant compensation network can be designed to integrate the output characteristics of SS and PS equivalent circuit topologies.

A. SS EQUIVALENT CIRCUIT TOPOLOGY

In order to achieve the above purpose, it is necessary to obtain the compensation capacitor C_{T0} that meets the topological resonance of the SS equivalent circuit and the compensation capacitor C_{f10} that meets the topological resonance of the PS circuit, respectively. By adjusting the corresponding coefficients K_{T} and K_{f1}, the output power becomes gentle with the variation trend of the coupling coefficient k, thereby obtaining the expected system anti-offset performance.

For the convenience of analysis and calculation, the branch composed of L_{T} and C_{T} can be defined as L_{E}:

$$j\omega L_{\mathrm{E}} = j\omega L_{\mathrm{T}} + \frac{1}{j\omega C_{\mathrm{T}}} \tag{17}$$

$$C_{\mathrm{T0}} = \frac{1}{\omega^2 L_{\mathrm{T}}} \tag{18}$$

B. PS EQUIVALENT CIRCUIT TOPOLOGY

When the PS equivalent circuit topology reaches resonance state, the value of compensation capacitor C_{f1} is C_{f10}. Therefore, the adjustment coefficient K_{T} is introduced to adjust the value of compensation capacitor C_{T}, so that the C_{T} at resonance of the equivalent PS circuit topology meets the following conditions: C_{T}=K_{T} C_{T0}, K_{T}>1. At this point, the equivalent input impedance of the PS circuit topology can be represented as:

$$\begin{aligned} Z_{\mathrm{in\_PS}} &= \frac{1}{j\omega C_{\mathrm{f10}}} // \left(j\omega L_{\mathrm{E}} + Z_{\mathrm{r0}} \right) \\ &= \frac{M^2 \omega^2 C_{\mathrm{f2}} L_{\mathrm{f2}} R_{\mathrm{eq}}}{{L_{\mathrm{f2}}}^2 \left(-1 + \omega^2 L_{\mathrm{E}} C_{\mathrm{f1}} \right)^2 + M^4 \omega^6 C_{\mathrm{f2}}^2 C_{\mathrm{f1}}^2 R_{\mathrm{eq}}^2} \\ &\quad + j \left(\frac{\omega L_{\mathrm{E}} {L_{\mathrm{f2}}}^2 - \omega^3 \left(L_{\mathrm{E}}^2 {L_{\mathrm{f2}}}^2 + M^4 \omega^2 C_{\mathrm{f2}}^2 R_{\mathrm{eq}}^2 \right) C_{\mathrm{f1}}}{M^4 \omega^6 C_{\mathrm{f1}}^2 C_{\mathrm{f2}}^2 R_{\mathrm{eq}}^2 + {L_{\mathrm{f2}}}^2 \left(-1 + \omega^2 L_{\mathrm{E}} C_{\mathrm{f1}} \right)^2} \right) \end{aligned} \tag{19}$$

When the imaginary part of the equivalent input impedance $Z_{\mathrm{in\_PS}}$ is 0 and exhibits pure resistance characteristics, the resonant state of the equivalent PS circuit topology can be achieved. At this point, the following equation is satisfied:

$$\mathrm{Im}\left(Z_{\mathrm{in\_PS}} \right) = \frac{\omega L_{\mathrm{E}} L_{\mathrm{f2}}^2 - \omega^3 \left({L_{\mathrm{E}}}^2 {L_{\mathrm{f2}}}^2 + M^4 \omega^2 C_{\mathrm{f2}}^2 R_{\mathrm{eq}}^2 \right) C_{\mathrm{f1}}}{M^4 \omega^6 C_{\mathrm{f1}}^2 C_{\mathrm{f2}}^2 R_{\mathrm{eq}}^2 + {L_{\mathrm{f2}}}^2 \left(-1 + \omega^2 L_{\mathrm{E}} C_{\mathrm{f1}} \right)^2} = 0 \tag{20}$$

The compensation capacitor C_{f10} and the equivalent inductance L_{E} meet the following equations:

$$C_{\mathrm{f10}} = \frac{L_{\mathrm{E}} L_{\mathrm{f2}}^2}{\omega^2 \left(M^4 \omega^2 C_{\mathrm{f2}}^2 R_{\mathrm{eq}}^2 + L_{\mathrm{E}}^2 L_{\mathrm{f2}}^2 \right)} \tag{21}$$

$$j\omega L_{\mathrm{E}} = j\omega L_{\mathrm{T}} + \frac{1}{j\omega K_{\mathrm{T}} C_{\mathrm{T0}}} \tag{22}$$

C. LCC CIRCUIT TOPOLOGY RESONANCE

Further considering the parameter L_{f1}, in order to meet the overall resonance state of the IPT system and make the input impedance Z_{in} exhibit pure resistance characteristics, an additional adjustment coefficient K_{f1} needs to be introduced to adjust the compensation capacitor C_{f1}, denoted as C_{f1}=K_{f1} C_{f10}, K_{f1}>1. At this point, the expression for Z_{in} is as shown in formula (23), at the bottom of the next page.

In order to exhibit pure resistance characteristics of Z_{in}, the following formula (24), as shown at the bottom of the next page, needs to be satisfied:

From the above equation, it can be seen that the value of compensation inductance L_{f1} is:

$$L_{\mathrm{f10}} = \frac{L_{\mathrm{E}} \left(-1 + \omega^2 L_{\mathrm{E}} C_{\mathrm{f1}} \right) L_{\mathrm{f2}}^2 + M^4 \omega^4 C_{\mathrm{f1}} C_{\mathrm{f2}}^2 R_{\mathrm{eq}}^2}{\left(-1 + \omega^2 L_{\mathrm{E}} C_{\mathrm{f1}} \right)^2 L_{\mathrm{f2}}^2 + M^4 \omega^6 C_{\mathrm{f1}}^2 C_{\mathrm{f2}}^2 R_{\mathrm{eq}}^2} \tag{25}$$

Meanwhile, the corresponding currents can be obtained as follows:

$$I_{\mathrm{Lf1}} = \frac{U_{\mathrm{p}}}{Z_{\mathrm{in}}} \tag{26}$$

$$I_{\mathrm{T}} = I_{\mathrm{Lf1}} \times \frac{\frac{1}{j\omega C_{\mathrm{f1}}}}{\frac{1}{j\omega C_{\mathrm{f1}}} + \left(\frac{1}{j\omega C_{\mathrm{T}}} + j\omega L_{\mathrm{T}} + Z_{\mathrm{r}} \right)} \tag{27}$$

$$I_{\mathrm{Cf1}} = I_{\mathrm{Lf1}} \times \frac{\frac{1}{j\omega C_{\mathrm{T}}} + j\omega L_{\mathrm{T}} + Z_{\mathrm{r}}}{\frac{1}{j\omega C_{\mathrm{f1}}} + \left(\frac{1}{j\omega C_{\mathrm{T}}} + j\omega L_{\mathrm{T}} + Z_{\mathrm{r}} \right)} \tag{28}$$

When the system resonates, ignoring the losses of each passive component, the power received by the reflection impedance equals the output power of the IPT system, which can be expressed as:

$$P_{\text{out}} = I_{\text{T}}^2 Z_{\text{r0}} \tag{29}$$

III. DESIGN OF BILATERAL LCC RESONANCE COMPENSATION NETWORK AND OPTIMIZATION OF SYSTEM ANTI-OFFSET PERFORMANCE

A. SETTING OF THE ADJUSTMENT COEFFICIENTS KT AND KF1 OF THE RESONANCE COMPENSATION NETWORK

Observing the bilateral LCC equivalent circuit and corresponding parameter formulas, it can be seen that the compensation network parameters are related to mutual inductance during system resonance. To study the impact of realtime mutual inductance between the receiving and transmitting coils on the system's anti offset ability and transmission performance, it is necessary to first assign values to the mutual inductance in the compensation network parameter expression, so the value of the circuit parameters L_{f1}, C_{f1}, and C_{T} represented by the adjustment coefficients K_{T} and K_{f1} are obtained. Therefore, it is necessary to first assume a virtual mutual inductance M_0 to determine the values of the parameters L_{f1}, C_{f1} and C_{T} on the primary side. The realtime mutual inductance value during the energy transmission process is M, which can be used to study the relationship between the output characteristics and the actual mutual inductance during the coil offset process. The system resonance configuration simulation parameter design is shown in Table 1 below:

The coupling coefficient operating range can be selected based on the variation relationship between the system output power P_{out} and the coupling coefficient k, the expected transmission efficiency η_{min}, and the standard output power P_{onorm} set for normal operating conditions. Therefore, it is necessary to propose the numerical values of the adjustment coefficients K_{T} and K_{f1} to determine the specific values of parameters L_{f1}, C_{f1}, and C_{T}, so as to study the variation of output power P_{out} with the coupling coefficient k and virtual mutual inductance M_0. Based on this, further select the value of virtual mutual inductance M_0 according to actual engineering needs, and obtain the variation pattern between power P_{out} and coupling coefficient k.

TABLE 1. Simulation parameters of bilateral LCC Type IPT system.

Parameters	Values
E / V	120
f / kHz	85
R_{eq} / Ω	10
L_{T} / μH	223
C_{R} / nF	19.37
L_{R} / μH	223
C_{f2} / nF	83.47
L_{f2} / μH	42

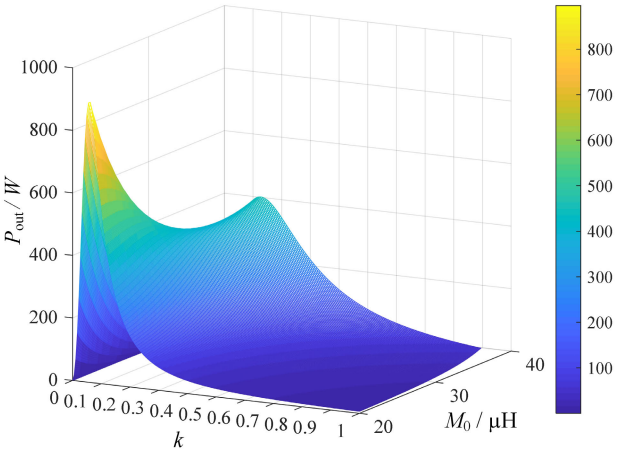

FIGURE 3. Varying surface of output power P_{out} with respect to the values of virtual mutual inductance M_0, coupling coefficient k.

Develop adjustment coefficients K_{T}=1.21 and K_{f1}= 1.3575, and study the variation rule between P_{out} and k when the virtual mutual inductance values M_0 are 20 μH, 24 μH, 28 μH, 32 μH, and 36 μH, respectively. Based on the above Figure 3, Figure 4 and formula, it can be seen that the values of different virtual mutual inductance M_0 correspond to different compensation parameters L_{f1}, C_{f1}, and C_{T} combinations, and the corresponding compensation parameters are different. The maximum output power P_{omax}

$$\begin{aligned} Z_{\text{in}} &= j\omega L_{\text{f1}} + (j\omega L_{\text{E}} + Z_{\text{r0}}) \,//\, \frac{1}{j\omega C_{\text{f1}}} \\ &= \frac{M^2\omega^2 C_{\text{f2}} L_{\text{f2}} R_{\text{eq}}}{M^4\omega^6 C_{\text{f1}}^2 C_{\text{f2}}^2 R_{\text{eq}}^2 + L_{\text{f2}}^2\left(-1+\omega^2 L_{\text{E}} C_{\text{f1}}\right)^2} \\ &\quad + j\frac{\omega\left(-1+\omega^2 L_{\text{E}} C_{\text{f1}}\right)\left(-L_{\text{f1}} + L_{\text{E}}\left(-1+\omega^2 L_{\text{f1}} C_{\text{f1}}\right)\right) L_{\text{f2}}^2 + M^4\omega^5 C_{\text{f1}} C_{\text{f2}}^2\left(-1+\omega^2 L_{\text{f1}} C_{\text{f1}}\right) R_{\text{eq}}^2}{\left(-1+\omega^2 L_{\text{E}} C_{\text{f1}}\right)^2 L_{\text{f2}}^2 + M^4\omega^6 C_{\text{f1}}^2 C_{\text{f2}}^2 R_{\text{eq}}^2} \end{aligned} \tag{23}$$

$$\text{Im}\left(Z_{\text{in}}\right) = \frac{\omega\left(-1+\omega^2 L_{\text{E}} C_{\text{f1}}\right)\left(-L_{\text{f1}} + L_{\text{E}}\left(-1+\omega^2 L_{\text{f1}} C_{\text{f1}}\right)\right) L_{\text{f2}}^2 + M^4\omega^5 C_{\text{f1}} C_{\text{f2}}^2\left(-1+\omega^2 L_{\text{f1}} C_{\text{fl}}\right) R_{\text{eq}}^2}{\left(-1+\omega^2 L_{\text{E}} C_{\text{f1}}\right)^2 L_{\text{f2}}^2 + M^4\omega^6 C_{\text{f1}}^2 C_{\text{f2}}^2 R_{\text{eq}}^2} = 0 \tag{24}$$

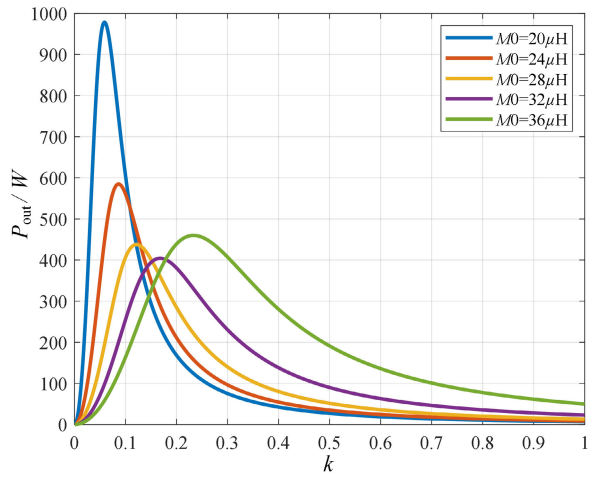

FIGURE 4. Variation curves of output power P_{out} with respect to coupling coefficient k with different values of mutual inductance M_0.

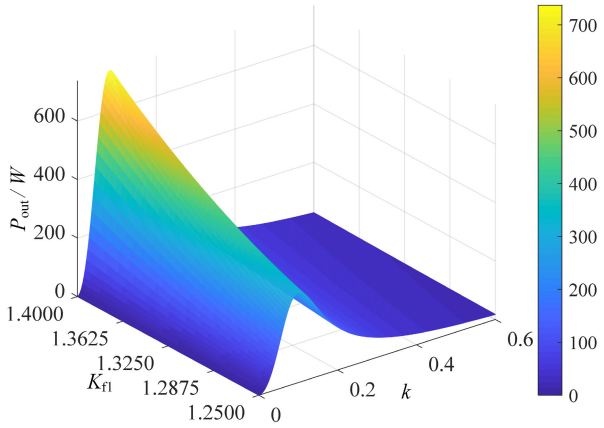

FIGURE 5. Varying surface of output power P_{out} with the adjustment coefficient K_{f1} and coupling coefficient k.

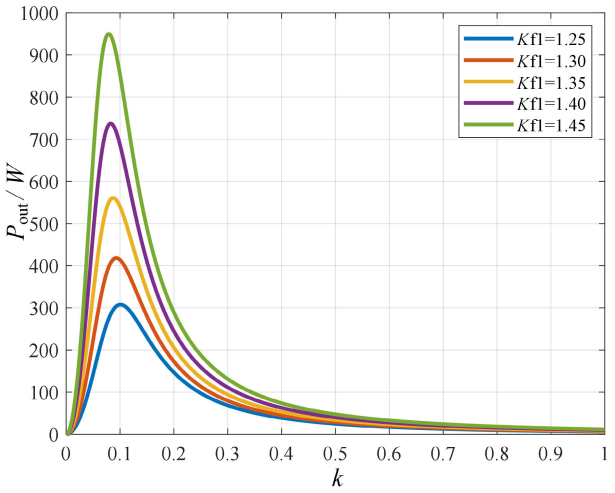

FIGURE 6. Varying curves of output power P_{out} with respect to coupling coefficient k for different adjustment coefficients K_{f1}.

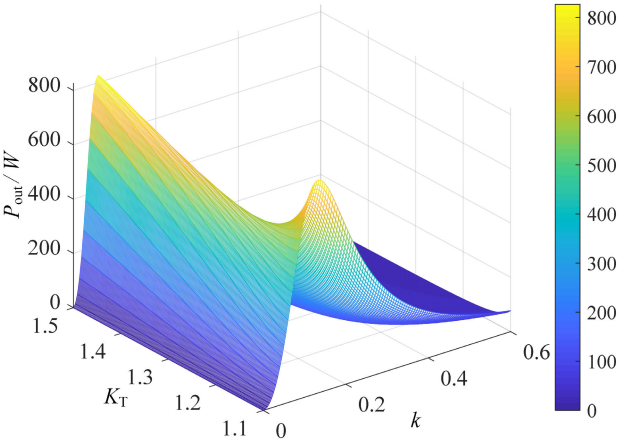

FIGURE 7. Varying curves of output power P_{out} with respect to coupling coefficient k for different adjustment coefficients K_{f1}.

shows a trend of first decreasing and then increasing with the increase of virtual mutual inductance value M_0, and its corresponding coupling coefficient k_{omax} has been continuously increasing. Therefore, this characteristic can be utilized to select the numerical value of virtual mutual inductance M_0 based on the required output performance and coupling range in actual engineering, and subsequently design the values of each compensation parameter.

To study the effects of the adjustment coefficients K_{f1} and K_T on the output power P_{out} during coil offset, the graph is drawn as follows:

As shown in Figure 5 and Figure 6, taking the virtual mutual inductance value M_0=24μH and the adjustment coefficient K_T=1.21, study the influence of the changes in the adjustment coefficient K_{f1} and coupling coefficient k on the output power P_{out}. Taking the adjustment coefficients K_{f1} as 1.25, 1.30, 1.35, 1.40 and 1.45 respectively, it can be observed that for each output power curve, as the coupling coefficient k increases, the system output power P_{out} gradually increases until the peak value P_{omax} and then slowly decreases. At the same time, as the value of the adjustment coefficient K_{f1} gradually increases, the output power P_{out} also increases with the same coupling coefficient value. In addition, the peak value of output power P_{omax} also increases, and the wave peak becomes steeper. The coupling coefficient k_{omax} corresponding to the peak value decreases with the increase of the adjustment coefficient K_{f1}.

As shown in Figure 7 and Figure 8, taking the virtual mutual inductance value M_0=24μH and the adjustment coefficient K_{f1}=1.3575, study the influence of the changes in the adjustment coefficient K_T and coupling coefficient k on the output power P_{out}. Taking the adjustment coefficients K_T as 1.10, 1.15, 1.20, 1.25 and 1.30 respectively, it can be observed that for each output power curve, as the coupling coefficient k increases, the output power P_{out} gradually increases until peak value P_{omax} is reached, and then slowly

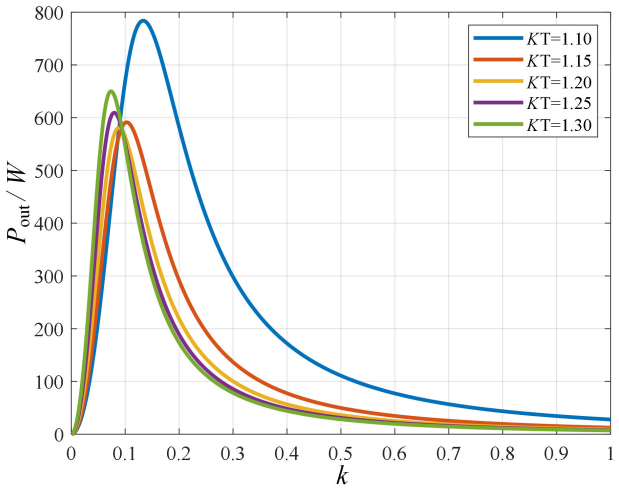

FIGURE 8. Varying curves of output power P_{out} with respect to coupling coefficient k for different adjustment coefficients K_{f1}.

decreases. At the same time, as the value of the adjustment coefficient K_T gradually increases, the peak value P_{omax} first decreases and then increases, and the coupling coefficient k_{omax} corresponding to its peak shows a decreasing trend with the increase of the adjustment coefficient K_T.

B. ESTABLISHMENT OF IPT SYSTEM LOSSY MODEL AND SELECTION OF ADJUSTMENT COEFFICIENTS K_T AND K_{F1}

In order to facilitate theoretical analysis and calculation, all passive components mentioned above are ideal devices. In practical engineering applications, it is necessary to consider the loss of the magnetic circuit mechanism, so as to balance the output power P_{out} and transmission efficiency η, provide better engineering basis for the selection of K_T and K_{f1}. The optimization design method mentioned in this article does not change the circuit topology, after considering internal resistance loss, when analyzing the relationship between P_{out} and virtual mutual inductance value M_0, coupling coefficient k, adjustment coefficient K_T, and K_{f1}, the variation pattern of output power before and after optimization is the same.

The main losses of the magnetic circuit mechanism are the internal resistance losses of the resonant coil and compensation inductance, in the equivalent circuit considering internal resistance loss, the equivalent internal resistance R_T of the Tx coil is connected in series with the resonant inductance L_T, and the equivalent internal resistance R_{Lf1} of the compensating inductance is connected in series with the compensating inductance L_{f1}. The equivalent internal resistance R_R of the Rx coil is connected in series with the resonant inductance L_R, and the equivalent internal resistance R_{Lf2} of the compensating inductance is connected in series with the compensating inductance L_{f2}. At this time, the circuit topology of the IPT system is shown in Figure 9, and the corresponding internal resistance is shown in Table 2 below.

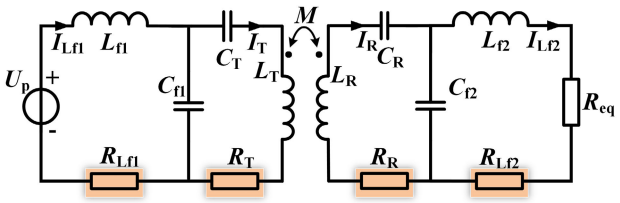

FIGURE 9. Simplified equivalent circuit diagram of the IPT system lossy mode.

TABLE 2. Internal resistance parameters of the bilateral LCC type IPT system lossy model.

Parameters	Values
R_T / Ω	0.065
R_{Lf1} / Ω	0.015
R_R / Ω	0.065
R_{Lf2} / Ω	0.013

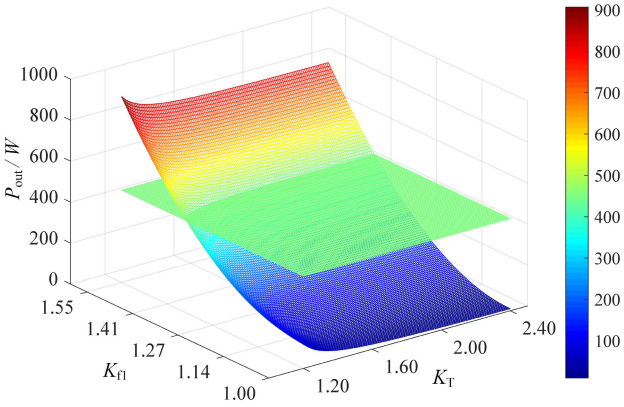

FIGURE 10. The relationship between power P_{out} and adjustment coefficient K_T and K_{f1}.

This article selects the virtual mutual inductance value M_0=24μH, and obtains the specific values of the parameters L_{f1}, C_{Lf1}, and C_T based on the system resonance conditions. Draw the varying surface of the output power P_{out} with respect to the adjustment coefficients K_T and K_{f1} when the actual mutual inductance M=27.23μH, furthermore, in order to achieve the target output power, the two-dimensional scatter plot of the transmission efficiency with respect to the adjustment coefficients K_T and K_{f1} is shown in Figure 10:

As shown in Figure 11, the two-dimensional scatter plot above shows the relationship between transmission efficiency η and the combination of adjustment coefficients K_T and K_{f1}, each scattering point represents the combination of various adjustment coefficients K_T and K_{f1} that can achieve the same numerical value of the target output power, where the color brightness represents the numerical value of transmission efficiency. The curved surface in the figure shows the changing trends of the output power P_{out} with the adjustment coefficients K_T and K_{f1} when no offset occurs. The plane represents the target output power P_{out}=450W, and the curve intersecting the plane and surface

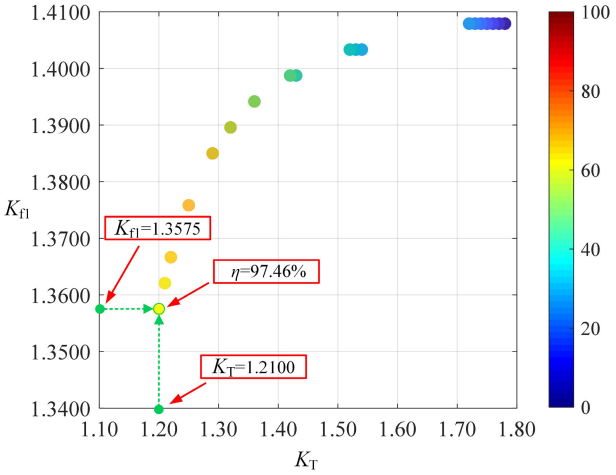

FIGURE 11. The relationship between the transmission efficiency η and the adjustment coefficients K_T and K_{f1}.

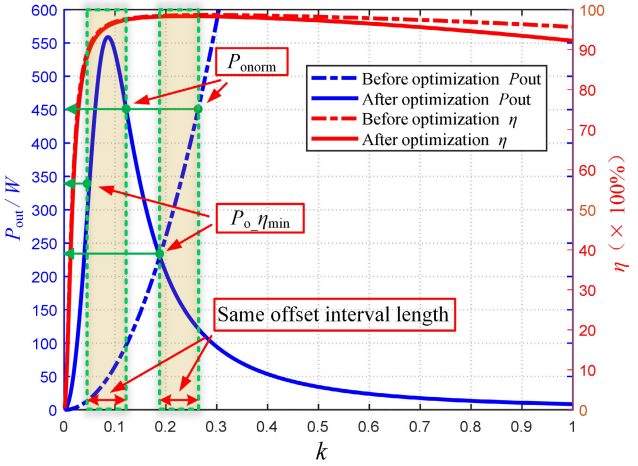

FIGURE 12. Before and after optimization, the variation curves of output power P_{out} and transmission efficiency η with coupling coefficient k.

represents the target output power that can be achieved by optimizing the circuit compensation parameters by adjusting the coefficients K_T and K_{f1}. Furthermore, based on the efficiency two-dimensional scatter plot, it can be seen that in order to achieve the target output power P_{out}=450W, among all the combinations of adjustment coefficients (K_T, K_{f1}) corresponding to the intersecting curve, when the adjustment coefficients K_T = 1.2100, K_{f1}=1.3575, the system can have the highest transmission efficiency η = 97.46%.

C. SELECTION OF COUPLING RANGE UNDER OFFSET CONDITIONS

In order to enable the IPT system to have relatively stable transmission performance within a certain range of mutual inductance changes and maintain high transmission efficiency, it is necessary to reasonably select the range of interval changes in the coupling coefficient k. The output power fluctuation degree of the IPT system within the coupling coefficient variety range depends on the absolute value of the maximum difference between the output power extreme value and the standard output power P_{onorm} within the entire coupling coefficient range, that is, the maximum deviation value ΔP_{abs_max}, the larger the value is, the greater the fluctuation of output power is. Therefore, it is necessary to first set the standard output power P_{onorm} of the system and its corresponding standard coupling coefficient k_{onorm} based on the actual working conditions, and use this as a basis to select the working range of the coupling coefficient.

When the virtual mutual inductance value M_0=24μH, the adjustment coefficient K_T=1.2100, K_{f1}=1.3575, the variation curves of output power P_{out} and transmission efficiency η with coupling coefficient k are shown below. In order to ensure that the system has a high transmission efficiency when offset occurs, this article sets the minimum transmission efficiency during the displacement process of the coupling mechanism η_{min}=90%, that is, inequality η_{min} always holds.

As shown in Figure 12, as the position of the coupling mechanism gradually shifts, the optimized system output power P_{out} will show a trend of first increasing and then decreasing as the parameter k decreases; The system output power P_{out} before optimization decreases monotonically as the parameter k decreases. In contrast, with the same coupling interval variation length, after optimization, the degree of decrease in output power P_{out} can be significantly reduced.

Based on the above Figure 12 and Table 3, set the required standard output power P_{onorm} =450W for the actual working conditions, as well as the corresponding to the coupling coefficient k_{onorm} =0.1221. Meantime, set the minimum transmission efficiency of the system η_{min}=90%,corresponding to the system output power $P_{o\_\eta min}$=340W, coupling coefficient $k_{o\_\eta min}$=0.0497. When offset occurs, the optimized system output power P_{out} gradually reaches the maximum value P_{omax} =559W, and the coupling coefficient k_{omax} at this time is 0.08592.Obviously, the range of coupling coefficient variation, before and after offset, $k \in$[0.0497, 0.1221], and the length of variation Δk_{max} = 0.0724.At the same time, the corresponding system drops from standard output power P_{onorm} =450W to $P_{o\_\eta min}$=340.0W, and the maximum deviation value of output power is ΔP_{abs_max} =P_{omax} - P_{onorm} =450.0-340.0=110.0W. Finally, it dropped to the original 75.56%. Before optimization, offset the same coupling interval length Δk_{max}=0.0724, that is, descending from the coupling coefficient k_{onorm} =0.2632 corresponding to the standard output power P_{onorm} to $k_{o\_\eta min}$=0.1908. The corresponding output power monotonically decreases from standard output power P_{onorm} = 450W to $P_{o\_\eta min}$=236.9W, ultimately decreases to the original 52.64%. The maximum deviation value of output power at this time is ΔP_{abs_max} = P_{onorm} -$P_{o\_\eta min}$ = 450-236.9=213.1W. After optimization, the maximum deviation value, after deviating

TABLE 3. Performance comparison of simulation experiments before and after optimization.

Design scheme	Before optimization		After optimization	
Deviation situation	When aligning	Maximum offset	When aligning	Maximum offset
P_{out} / W	450.0	236.9	450.0	340.0
k	0.2632	0.1908	0.1221	0.0497
η	98.65%	98.47%	97.42%	90.00%
P_{omax} / W	450.0W		559.0W	
ΔP_{abs_max} / W	213.1		110.0	
Δk_{max}	0.0724		0.0724	

the same coupling interval length, ΔP_{abs_max} decreased from 213.1W before optimization to 110.0W after optimization, a decrease of 48.38%, effectively suppressing the fluctuation of output power; Meanwhile, the output power after deviation increased from 236.9W before optimization to 340.0W after optimization, an increase of 43.52%. At the same time, the system can still maintain a transmission efficiency of 90%.

IV. ANALYSIS AND OPTIMIZATION OF ANTI-OFFSET PERFORMANCE BASED ON 4DQ COILS

A. INTRODUCTION TO THE STRUCTURE OF 4DQ COIL

As shown in Figure 13, the coil used in this article is a 4DQ coil magnetic circuit mechanism. The 4D coil is a bipolar planar coil winding, which can increase the anti-offset performance in the X-axis and Y-axis directions. Using the same Leeds wire to wind a Q coil can enhance the coupling ability in the vertical Z-axis direction. In this way, it can ensure the anti-offset performance in the plane direction and increase the energy coupling in the transmission direction. Combining the structural schematic Figure 13 and the magnetic field distribution cloud Figure 14, it can be seen that when the receiving coil deviates along the X-axis or Y-axis direction, the net magnetic flux of the 4D coil passing through the Q coil on the opposite side is zero. The energy coupling between the 4D coil windings on both sides and between the Q coil windings on both sides are independent of each other and does not affect each other. Based on this, this magnetic circuit coupling mechanism is selected in this article. The following Table 4 shows the specific parameters and coil structure diagram of the magnetic coupling mechanism.

B. MAGNETIC FIELD CLOUD MAP OF 4DQ COIL

As shown in Figure 14, as the net magnetic flux flowing through each other's coils generated by the 4D and Q windings respectively is zero, the magnetic flux cross chain generated by the 4D and Q windings does not affect each other, and can achieve independent energy transfer and meet the decoupling characteristics.

V. DESIGN AND VERIFICATION OF EXPERIMENTAL PROTOTYPES

This section builds a prototype model of the IPT system based on the basic parameters in the Table 5 below and the proposed circuit parameter optimization scheme, and studies the anti-offset performance of the bilateral LCC topology IPT system based on 4DQ coils.

A. SETUP OF THE IPT SYSTEM

The experimental prototype is shown in Figure 15, in actual working conditions, as the position deviation of AGV mainly occurs in the horizontal plane direction, this article does not consider the displacement of the Z-axis direction. In the prototype experiment, it is more intuitive and operational to study the impact of spatial position deviation of the coils on the system anti deviation ability and transmission characteristics. In order to verify the feasibility and effectiveness of the optimization design scheme for the anti-offset performance of the IPT system, as shown in Figure 16, the following is a point-and-figure chart of P_{out} and η, before and after optimization, as the magnetic circuit mechanism shifts along the X/Y axis direction in a certain step size.

During the displacement process of the coupling mechanism, the mutual inductance value corresponding to every 20mm step offset is measured using an impedance analyzer, and the values of the input power of the *Tx* side, the output power of the *Rx* side, as well as the corresponding transmission efficiency are measured through a power analyzer. Due to the presence of certain losses in the switch tubes and passive components, and the inevitable errors in configuring the resonant network, the actual transmission performance of the system is slightly worse than the theoretical value. The relationship between mutual inductance and system transmission performance can be referred to formulas (6), (27) and (29) above. Analyzing the above figure, it can be seen that the target output power before optimization is 427.6W. Due to the deviation, the output power and transmission efficiency rapidly decrease; In order to meet the needs of engineering applications and maintain the target output power of the same value, when the same offset coupling interval occurs, the output power of the optimized IPT system first increases and then decreases, that is, the fluctuation degree of output power within the unit offset distance decreases, at the same time, the overall decrease in transmission efficiency after optimization has eased. In addition, when the offset distance is less than 120mm, although the optimized transmission efficiency is slightly lower than the transmission efficiency before optimization, when the offset distance is large enough, that is, when it is larger than 120mm, the output power and transmission efficiency of the system are better than before.

TABLE 4. Performance comparison of simulation experiments before and after optimization.

4DQ Coil	Wire diameter d / mm	Liz Line Specifications	Turn spacing / mm	Length * width / mm*mm	Turns of 4D winding	Turns of Q winding
Values	3.96	0.1*800	4.96	450*450	10	10

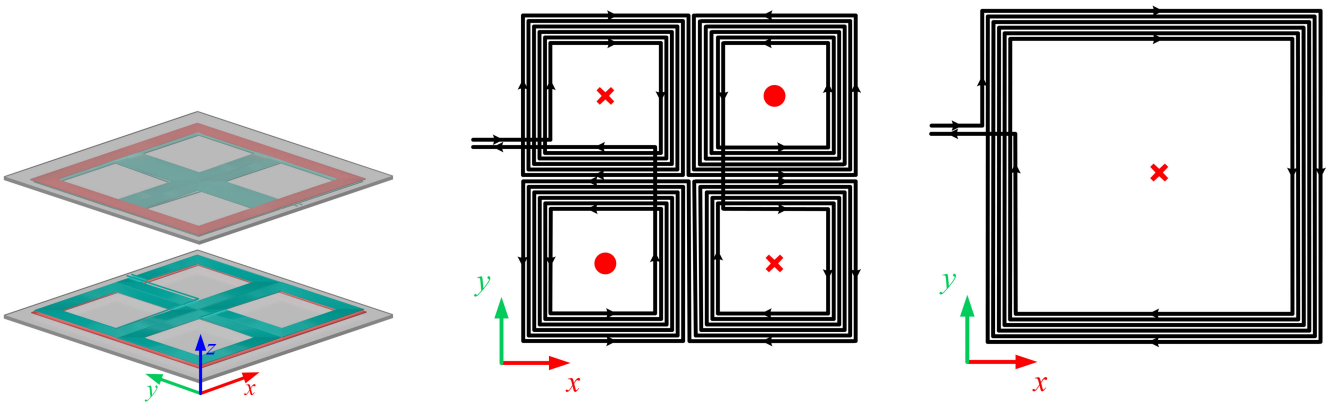

(a) (b) (c)

FIGURE 13. Schematic diagram of 4DQ coil structure. (a) Elevation view of 4DQ coil; (b) Vertical view of 4D winding; (c) Vertical view of Q winding.

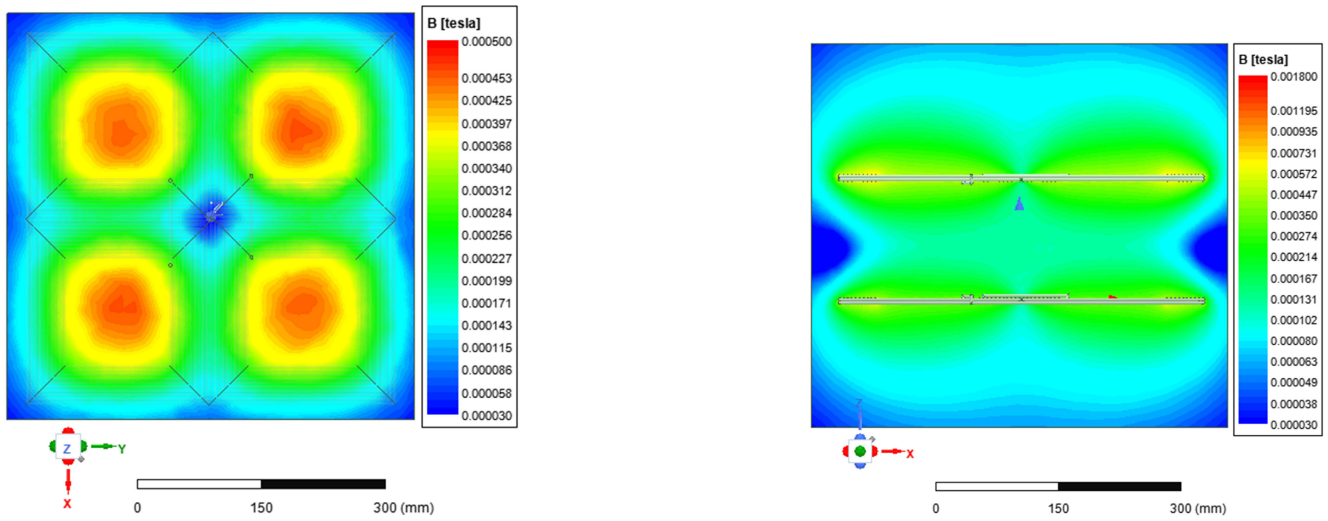

(a) (b)

FIGURE 14. Magnetic field energy distribution diagram of 4DQ coil. (a) Vertical view of 4D coil magnetic field distribution; (b) Front view of 4DQ coil magnetic field distribution.

TABLE 5. Performance comparison of simulation experiments before and after optimization.

Primary side parameters	Before optimization	After optimization	Secondary side parameters	before and after optimization
R_T/ Ω	0.32	0.32	R_R/ Ω	0.345
L_T/ μH	215.20	215.20	L_R/ μH	219.47
C_T/ nF	20.53	20.437	C_R/ nF	20.43
R_{Lf1}/ Ω	0.166	0.303	R_{Lf2}/ Ω	0.1928
L_{Lf1}/ μH	44.39	73.99	L_{Lf2}/ μH	47.62
C_{f1}/ nF	78.70	100.7	C_{f2}/ nF	73.23
E / V	140		R_L/ Ω	30

B. EXPERIMENTAL WAVEFORMS

As shown in Figure 17, in order to improve the anti-offset performance, the compensation parameters of the bilateral LCC network topology were optimized. The transmission performance is shown below.

When the coils are aligned, the input waveforms of the *Tx* side, the output waveforms of the *Rx* side, and the relevant data of the corresponding power analyzer are as follows:

As shown in Figure 18, after offset, the input waveforms of the *Tx* side, the output waveforms of the *Rx*

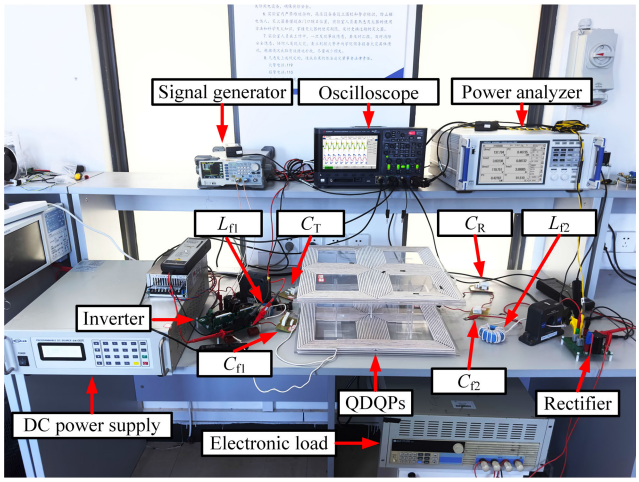

FIGURE 15. Bilateral LCC type magnetic coupling experimental prototype with anti-offset performance.

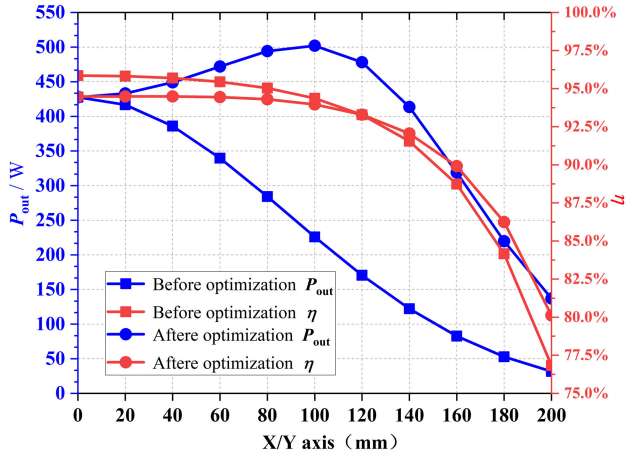

FIGURE 16. Bilateral LCC type magnetic coupling experimental prototype with anti-offset performance.

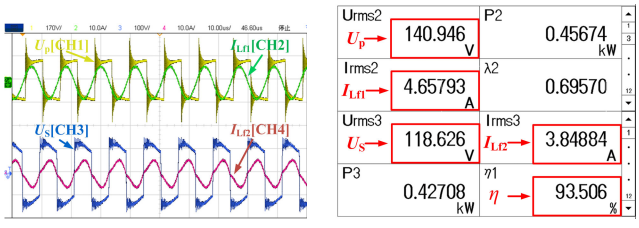

(a) (b)

FIGURE 17. After optimization, the waveforms and corresponding data when the coupling mechanism is directly aligned, where the coupling coefficient k=0.1862.

side, and the relevant data of the corresponding power analyzer:

Based on the waveforms and power analysis data, it can be seen that, to meet the requirements of engineering applications, the optimized bilateral LCC network topology IPT system has an output power of 427.08W without

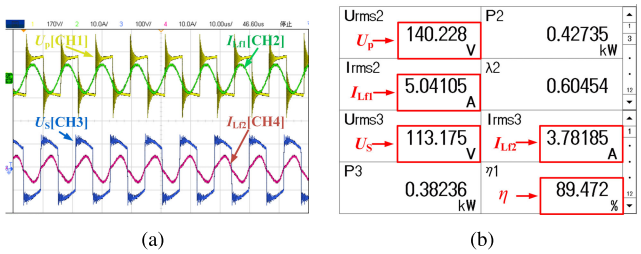

(a) (b)

FIGURE 18. The waveforms and corresponding data when the transmission efficiency η=89.472%, where the coupling coefficient k=0.0929.

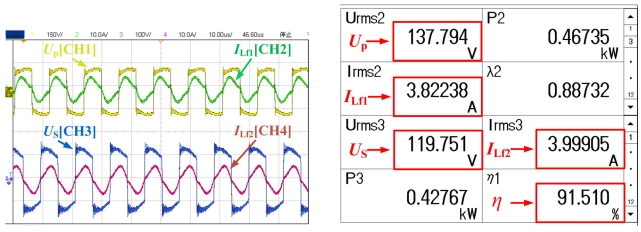

(a) (b)

FIGURE 19. Before optimization, the waveforms and corresponding data when the coupling mechanism is directly aligned, where the coupling coefficient k=0. 1594.

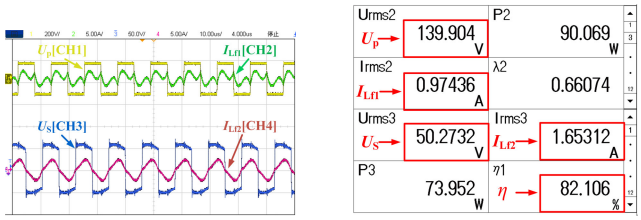

(a) (b)

FIGURE 20. Before optimization, the waveforms and corresponding data when the coupling mechanism is directly aligned, where the coupling coefficient k=0. 1594.

any offset, and the actual transmission efficiency of the corresponding system is 93.506%; The output power after offset is 382.36W, and the corresponding actual transmission efficiency is 89.472%. Before and after the offset, the output power decreased by 44.72W, with a coupling coefficient variation range of [0.0929, 0.1862], and an interval length of $\Delta\ k$=0.0933, resulting in a 4.034% decrease in efficiency. In contrast, the unoptimized IPT system starts with the same target output power of 427W, and the offset coupling coefficient interval length is also 0.0933, its system performance is shown in Figure 19 below. The input waveforms of the *Tx* side, output waveforms of the *Rx* side, and relevant data of the power analyzer are as follows:

As shown in Figure 20, after offsetting the same length of the coupling coefficient interval $\Delta\ k$=0.0933=0.0933, the input waveforms of the *Tx* side, the output waveforms of the *Rx* side, and the relevant data of the corresponding power analyzer are as follows:

Based on the waveforms and power analysis data, it can be seen that, the unoptimized bilateral LCC network topology IPT system has an output power of 427.67W without any offset, and the actual transmission efficiency is 91.51%; after offsetting the same length of the coupling coefficientinterval $\Delta\ k$=0.0933, the output power is 73.952W and the corresponding actual transmission efficiency is 82.106%.Before and after the offset, the output power decreased by 353.718W, with a coupling coefficient variation range of [0.0661,0.1594], resulting in a 9.404% decrease in efficiency.

VI. CONCLUSION

Regarding the issue of the coil misalignment during AGV wireless power transmission, this paper proposes an optimization design method based on the parameters of a bilateral LCC resonant compensation network. This method introduces two adjustment coefficients K_{T} and K_{f1} to optimize the design of the compensation capacitors C_{T} and C_{f1} on the *Tx* side of the LCC circuit, respectively. Based on the efficient transmission of the system as a limiting condition, the system can achieve suppression of output power fluctuations within a wider range of coupling coefficient variations. Finally, the anti-offset performance of the proposed scheme was verified through an experimental prototype with an output power of 427W, the optimized coupling mechanism maintains a transmission efficiency of 89.472% or above when offset to 153mm, i.e., within the range of 0-34% lateral/longitudinal offset percentage, while achieving the maximum deviation value of output power $\Delta\ P_{\mathrm{abs\_max}}$ decreased from 213.1W before optimization to 111.0W after optimization, a decrease of 47.91%, effectively suppressing the output power fluctuation of the system.

REFERENCES

[1] C. Zhu, J. Yu, Y. Gu, J. Gao, H. Yang, R. Mai, Y. Li, and Z. He, "Analysis and design of cost-effective WPT systems with dual independently regulatable outputs for automatic guided vehicles," *IEEE Trans. Power Electron.*, vol. 36, no. 6, pp. 6183–6187, Jun. 2021.

[2] S.-J. Huang, T.-S. Lee, W.-H. Li, and R.-Y. Chen, "Modular on-road AGV wireless charging systems via interoperable power adjustment," *IEEE Trans. Ind. Electron.*, vol. 66, no. 8, pp. 5918–5928, Aug. 2019.

[3] S. Z. Yang and Z. Y. Xia, "Non-blind zone mod method based on incomplete compensation of detection coil for EV wireless charging system," *Proc. CSEE*, vol. 42, no. 20, pp. 7363–7375, Oct. 2022.

[4] R. Tavakoli, E. M. Dede, C. Chou, and Z. Pantic, "Cost-efficiency optimization of ground assemblies for dynamic wireless charging of electric vehicles," *IEEE Trans. Transport. Electrific.*, vol. 8, no. 1, pp. 734–751, Mar. 2022.

[5] L. Tan, Z. Tang, R. Zhong, X. Huang, H. Liu, and C. Chen, "An optimization strategy based on dimension reduction method in wireless charging system design," *IEEE Access*, vol. 7, pp. 151733–151745, 2019.

[6] C. Rakluea, A. Worapishet, S. Chaimool, Y. Zhao, and P. Akkaraekthalin, "True nulls-free magnetoinductive waveguides using alternate coupling polarities for batteryless dynamic wireless power transfer applications," *IEEE Trans. Power Electron.*, vol. 37, no. 8, pp. 8835–8854, Aug. 2022.

[7] S. Cui, B. Song, and Z. Wang, "Overview of magnetic coupler for electric vehicles dynamic wireless charging," *Trans. China Electrotech. Soc.*, vol. 37, no. 3, pp. 537–554, 2022.

[8] W. Lihao and Z. Bo, "Overview of static wireless charging technology for electric vehicles: Part I," *Trans. China Electrotech. Soc.*, vol. 35, no. 6, pp. 1153–1165, 2020.

[9] R. Tavakoli, T. Shabanian, E. M. Dede, C. Chou, and Z. Pantic, "EV misalignment estimation in DWPT systems utilizing the roadside charging pads," *IEEE Trans. Transport. Electrific.*, vol. 8, no. 1, pp. 752–766, Mar. 2022.

[10] Y. Yao, Y. Wang, X. Liu, Y. Pei, and D. Xu, "A novel unsymmetrical coupling structure based on concentrated magnetic flux for high-misalignment IPT applications," *IEEE Trans. Power Electron.*, vol. 34, no. 4, pp. 3110–3123, Apr. 2019.

[11] Y. Chen, R. Mai, Y. Zhang, M. Li, and Z. He, "Improving misalignment tolerance for IPT system using a third-coil," *IEEE Trans. Power Electron.*, vol. 34, no. 4, pp. 3009–3013, Apr. 2019.

[12] C. Rong, X. He, M. Liu, Y. Wang, X. Liu, C. Lu, Y. Zeng, and R. Liu, "Omnidirectional free-degree wireless power transfer system based on magnetic dipole coils for multiple receivers," *IEEE Access*, vol. 9, pp. 81588–81600, 2021.

[13] J. W. Wang, "Review of research on compensation topologies for inductively coupled power transfer systems under variable parameters conditions," *Proc. CSEE*, vol. 42, no. 20, pp. 7288–7306, Oct. 2022.

[14] Y. Chen, B. Yang, Q. Li, H. Feng, X. Zhou, Z. He, and R. Mai, "Reconfigurable topology for IPT system maintaining stable transmission power over large coupling variation," *IEEE Trans. Power Electron.*, vol. 35, no. 5, pp. 4915–4924, May 2020.

[15] Z. B. Wang, "Three-coil wireless power transfer system with constant output power and constant transfer efficiency characteristics," *Proc. CSEE*, vol. 42, no. 20, pp. 7332–7343, Oct. 2022.

[16] Y. Yao, Y. Wang, X. Liu, Y. Pei, D. Xu, and X. Liu, "Particle swarm optimization-based parameter design method for S/CLC-compensated IPT systems featuring high tolerance to misalignment and load variation," *IEEE Trans. Power Electron.*, vol. 34, no. 6, pp. 5268–5282, Jun. 2019.

[17] K. Li, H. Yuan, S.-C. Tan, and S. Y. R. Hui, "Overshoot damping and dynamics improvement in wireless power transfer systems via receiver-side controller design," *IEEE Trans. Power Electron.*, vol. 37, no. 2, pp. 2362–2371, Feb. 2022.

[18] S. Song, Q. Zhang, Z. He, H. Li, and X. Zhang, "Uniform power dynamic wireless charging system with I-type power supply rail and DQ-phase-receiver employing receiver-side control," *IEEE Trans. Power Electron.*, vol. 35, no. 10, pp. 11205–11212, Oct. 2020.

[19] H. Niu, G. Li, J. Lu, and X. Pan, "Parameter identification method with dynamic impedance modulation for the DWPT system," *IEEE J. Emerg. Sel. Topics Power Electron.*, vol. 10, no. 5, pp. 6332–6344, Oct. 2022.

[20] C. Xia, X. Li, X. Han, X. Yang, X. Li, and Z. Liao, "A hybrid control method for achieving constant voltage output with LADR efficiency tracking for IPT systems," *Proc. CSEE*, vol. 42, no. 5, pp. 6042–6052, 2022.

[21] S. Li, L. Wang, Y. Guo, and Z. Liu, "Flexible energy-transfer control of dynamic wireless power transfer system based on estimation of load and mutual inductance," *IEEE Trans. Ind. Appl.*, vol. 58, no. 1, pp. 1157–1167, Jan. 2022.

YANG LU was born in Zhoushan, Zhejiang, China, in 1992. He received the B.Eng. degree in electrical engineering and automation from Southeast University, Nanjing, China, in 2015, and the M.Eng. degree in electrical engineering from Northeast Electric Power University, Jilin, China, in 2019. He is currently pursuing the Ph.D. degree with the China University of Mining and Technology, Xuzhou, China.

His main research interests include wireless power transmission, automated guided vehicle battery chargers, technique of power electronics and power transmission, and photovoltaic energy storage.

DONGYUAN GE was born in Qingyuan, Baoding, Hebei, China, in 1978. She received the B.S. degree in computers and applications and the M.S. degree in project management from the Harbin Institute of Technology, Harbin, in 2000 and 2013, respectively.

She is currently a Senior Engineer and majored in the artificial intelligence and data governance. Since 2022, she has been the Head of the Data Center, State Grid Heilongjiang Information & Telecommunication Company Ltd. She is mainly responsible for organizing the research of big data products and project management.

LIAN MENG was born in Xinye, Henan, in 1991. He received the bachelor's degree in electronic information engineering from Daqing Normal University, in 2016, and the master's degree in information and communication engineering from Northeast Electric Power University, in 2016.

From 2019 to 2023, he worked in information and communication operations with State Grid Fuyang Power Supply Company. Since 2018, he has published six articles and owns over ten patents. His research interests include the study and application of intelligent algorithms and research on wireless transmission technologies.

CHUAN SUN was born in Zibo, Shandong, in 1982. He received the master's degree in communication and information systems from the Taiyuan University of Technology, in 2010.

In July 2010, he joined State Grid Fuyang Power Supply Company and has been engaged in power communication work ever since. Since 2015, he has been successively obtained the qualifications of transmission mechanic technician and a Senior Engineer in electrical engineering technology. He has published more than 30 articles and obtained two patents. His main research interests include the application of power communication and system maintenance.

QI TANG was born in Jilin City, Jilin, China, in 1993. He received the B.S. degree in communication engineering from the University of Beihua, Jilin, in 2016, and the M.S. degree in information and communication engineering from Northeast Electric Power University, Jilin, in 2020.

He is currently an Assistant Engineer and majored in wireless sensor networks. Since 2020, he has been with State Grid Heilongjiang Information & Telecommunication Company Ltd., and State Grid Anhui Electric Power Company Ltd.

YILIN GAO was born in Shangqiu, Henan, China, in 2000. She received the bachelor's degree in management from the Hubei University of Economics, Wuhan, China, in 2023. She is currently pursuing the Ph.D. degree. Her research interests include the design and modeling of wireless power transfer with relay coils, multi-objective optimization algorithm, and other optimization algorithms.

MENGMENG CHEN was born in Shangqiu, Henan, China, in 2000. He received the B.Eng. degree in electrical engineering and automation from the China University of Mining and Technology, Xuzhou, China, in 2022, where he is currently pursuing the M.Eng. degree with the School of Electrical Engineering.

His current research interests include the design and modeling of wireless power transfer with relay coils and unmanned aerial vehicles battery chargers.

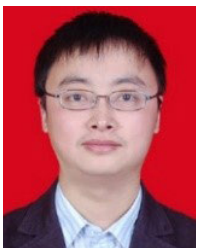

CHENYANG XIA was born in Jiangsu, China, in 1982. He received the B.S., M.S., and Ph.D. degrees in control theory and control engineering from Chongqing University, Chongqing, China, in 2006, 2008, and 2010, respectively.

From 2018 to 2019, he was an Academic Visitor with the University of Auckland, Auckland, New Zealand. He is currently a Professor with the School of Electrical Engineering, China University of Mining and Technology, Xuzhou, China. His research interests include wireless power transfer and intelligent control.